
Article:
Henson, Benjamin, Shen, Lu and Zakharov, Yury orcid.org/0000-0002-2193-4334 (2022) Full-duplex UAC receiver with two-sensor transducer. IEEE Transactions on Circuits and Systems II: Express Briefs. pp. 4764-4768. ISSN: 1549-7747

https://doi.org/10.1109/TCSII.2022.3199030

Full-duplex UAC receiver with two-sensor transducer

Benjamin Henson, *Member, IEEE*, Lu Shen, *Member, IEEE*, Yuriy Zakharov, *Senior Member, IEEE*

***Abstract*—In this brief we present a design of a full-duplex (FD) underwater acoustic communication (UAC) receiver with a two-sensor transducer. The transducer consists of two piezo-ceramic cylinders cast together in polyurethane resin; one acts as a hydrophone and the other a projector. As the distance between the projector and hydrophone is extremely short, a high level of self-interference (SI) from the projector is received at the hydrophone. This SI must be eliminated to enable far-end data demodulation. In this work, we adopt a digital SI cancellation scheme based on adaptive filtering. We investigate the SI cancellation and far-end data demodulation performance with the two-sensor transducer in tank and lake experiments. The Rake receiver is used for the far-end data demodulation. As demonstrated by the experimental results, the far-end SNR loss in the FD experiment is less than 3 dB compared to the half-duplex experiment when there is only far-end transmission.**

***Index Terms*—Acoustic sensor, digital cancellation, full-duplex, self-interference, underwater acoustics**

I. Introduction

UNDERWATER acoustic communication (UAC) suffers from limited frequency bandwidth for data transmission [1]. To increase the capacity of the communication channel, we consider full-duplex (FD) UAC where the transducer can simultaneously transmit and receive in the same frequency bandwidth [2], [3]. In this work, a two-sensor transducer with two piezo-ceramic cylinders is presented for FD UAC systems, one cylinder is intended to operate as a projector (Tx) and the other one as a hydrophone (Rx). The overall size of the transducer is comparable to that of a conventional design with a single sensor. With such a compact transducer design, the projector and hydrophone are extremely close to each other. In such a case, the near-end self-interference (SI) from the projector is significantly stronger than the far-end signal arrived at the hydrophone.

The main challenge here is to cancel the near-end SI to the receiver's noise floor. This might seems straightforward, if one knows the near-end transmitted signal, it can be subtracted from the received signal and what is left is the 'far-end' signal of interest plus the noise. In practice, this task is difficult as it requires high-accuracy estimates of the SI propagation channel together with the hardware imperfections in the transmit and receive chains [4]. Apart from the strong direct path from the projector through the polyurethane (PU) resin to the hydrophone, there are multiple time-varying paths where the sound has entered the water and reflected off of nearby objects and/or boundaries such as the water's surface [5]–[7]. Any uncancelled SI will be added to the noise, thus reducing the far-end signal to noise ratio (SNR). Passive SI cancellation, such as shielding techniques in the acoustic domain can be applied to reduce the acoustic energy transferred from the projector to the hydrophone [8]. However, it would also reduce the power of the far-end desired signal received by the hydrophone. In our design, no acoustic baffle or physical isolation is inserted between the projector and hydrophone. SI cancellation can also be implemented in the analogue domain. Indeed, in radio FD applications this is essential due to the limited dynamic range of the analogue-to-digital converters (ADCs) available at radio communication frequencies [9]–[11]. However, at acoustic communication frequencies, which are significantly lower, high resolution ADCs ($\geq$ 24 bits) are available [12]. This means that it is feasible to implement entirely digital cancellation up to such high levels. Therefore, digital cancellation is often considered as the main approach for SI cancellation in FD UAC systems [13]–[16]. In [14], an over-parameterization based recursive least squares (RLS) algorithm with a sparsity constraint was proposed for digital cancellation. The performance of the FD UWA system is evaluated in an anechoic water tank. A bit error rate (BER) of 0.03 is achieved when the SI signal is 20 dB stronger than the far-end desired signal. In [15], a maximum likelihood algorithm with a sparsity constraint was proposed. Its performance was evaluated in the same water tank experiment as described above. A BER of 0.005 can be achieved when the SI signal is 50 dB higher than the far-end signal and the BER performance starts to degrade at higher SI levels. However, in practice, the near-end SI level could be much stronger and the fast SI channel variation must be taken into account.

One of the factors limiting the digital cancellation performance is the nonlinearity introduced by the power amplifier (PA). It is found in [16] that the influence of the nonlinear distortions introduced by the PA on the cancellation performance can be significantly reduced by using the digitalized PA output as the reference signal. With that taken into account, in time-invariant scenarios, the SI signal can be removed from the hydrophone signal with a residual signal level close to the receiver's noise floor using classical RLS adaptive filters [16]. In our lake experiments, more advanced adaptive filtering algorithms will be used to track the SI channel variation caused by reflections from the time-varying lake surface [6], [17]. We investigate the performance of a UAC system with spread-spectrum signals. After the SI cancellation, a Rake

B. Henson and L. Shen contributed equally to this work. The authors are with Department of Electronic Engineering, University of York, U.K. (e-mail: benjamin.henson@york.ac.uk; lu.shen@york.ac.uk; yury.zakharov@york.ac.uk). This work was supported in part by the U.K. EPSRC through Grants EP/V009591/1 and EP/R003297/1.

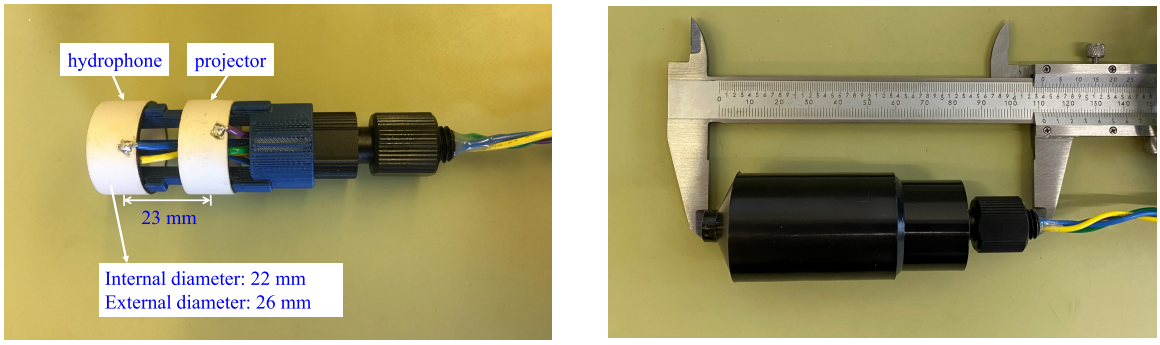

(a) The piezo-ceramics before being cast in PU resin.

(b) The transducer after casting.

Fig. 1: The two-sensor transducer.

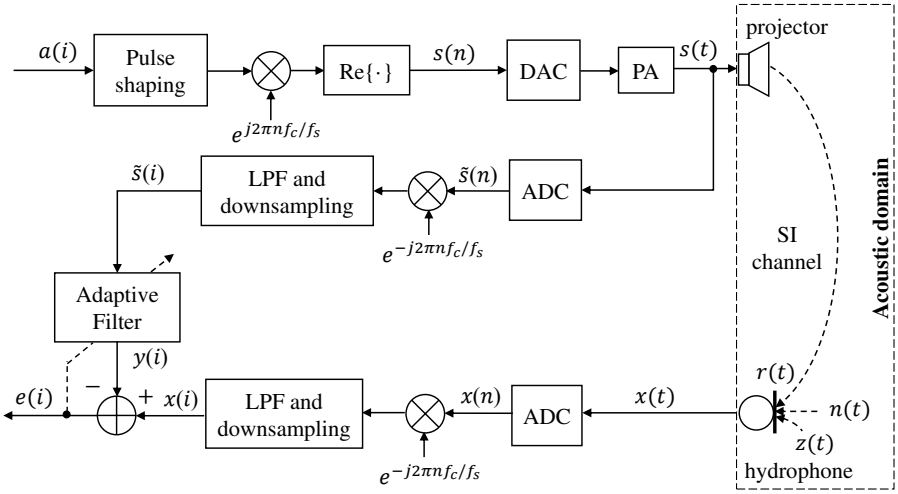

Fig. 2: Block diagram of the SI cancellation system [16], where index n and i denotes signal samples at a high sampling rate f_s and a low sampling rate f_d, respectively.

receiver [18] is used to deal with the multipath interference in the far-end channel. Results indicate that the demodulation performance of the receiver in FD experiments is close to that in a half-duplex experiment where only the far-end signal is transmitted. Note that although the digital cancellation is used as the main approach for SIC in the proposed design, a combination of SIC in multiple domains is also considered for future designs. For example, by combining SIC technique in the acoustic domain [19] with digital SI cancellation, there is a potential of achieving a much higher level of SIC.

In this paper we present a two-sensor transducer design for FD UAC systems. The digital cancellation performance of the system is evaluated in tank and lake experiments. The demodulation performance of the receiver is investigated and compared in half-duplex and FD modes. Both the digital cancellation and far-end data demodulation are done offline using the recorded data. Section II describes the transducer. The digital SI cancellation scheme is presented in Section III. Section IV presents the experimental results and Section V draws conclusions.

II. Two-sensor transducer

The transducer consists of two piezo-ceramic cylinders from Steiner & Martins Inc. USA [20] (part number SMC26D22H13111) of 22 mm and 26 mm internal and external diameters and the height of 13 mm. The resonant frequency is around 42 kHz. The ceramics were mounted on a 3D printed frame that held them in position on an aluminium fixing during the casting process. The material for the 3D print was acrylonitrile styrene acrylate (ASA). Photographs of the piezo-ceramics before being cast in PU resin and the final transducer are shown in Fig. 1. ASA and PU have relative densities (re water) of 1.08 and 1.18, respectively. These values mean that there will be reflections at the material boundaries, however, because these multipaths are static, they can be sucessfully dealt with in the digital SI cancellation. Using a noise-like signal at a carrier frequency of $f_c = 24$ kHz and 4 kHz bandwidth, a comparison was made with a known hydrophone and projector, the receive sensitivity was measured to be approximately -175 dB re V/μPa, and the transmit sensitivity to be approximately 103 dB re μPa/V@1m.

III. Digital SI cancellation

The block diagram of the digital SI cancellation system is shown in Fig. 2. The system operates at two sampling rates, a high sampling rate f_s is used for signal reception and a lower sampling rate f_d is used for the adaptive filtering. The transmitted symbols $a(i)$ are generated digitally, passed through a

root-raised cosine (RRC) filter for pulse-shaping [18], and then up-converted to the passband. The passband signal $s(n)$ is the input to the digital-to-analogue converter (DAC) whose output analogue signal drives the PA. This, in turn, drives the piezo-ceramic transmitter projector. The acoustic signal then passes through the PU resin to the receiver hydrophone via a direct acoustic path. Apart from the direct path SI, the acoustic SI signal also includes multiple reflections from the water surface, bottom and nearby objects.

The hydrophone converts the received acoustic signal into an electrical signal $x(t)$ that is then digitalized using the ADC, low-pass filtered (LPF) and down-sampled to the low sampling rate f_d. This signal is used as the desired signal of the adaptive filter. The LPF is implemented using the RRC filter, the same as in the transmitter. The PA output went through the same processing, and its lower sampling rate version is used as the regressor of the adaptive filter. The task of the adaptive filter is to produce filter coefficients that represent the impulse response of the analogue and acoustic paths between the projector and hydrophone. In time-invariant scenarios, the classical RLS adaptive filter would be sufficient for the digital SI cancellation. In time-varying scenarios, adaptive filtering algorithms with a better tracking ability are required to cancel the SI to the noise floor [6], [17]. The parameters of the adaptive filter need to be adjusted for each scenario to achieve the best SIC performance.

IV. Experimental results

In subsection IV-A, the digital SI cancellation performance with the two-sensor transducer is investigated. Subsection IV-B investigates the demodulation peformance of the receiver in half-duplex and FD lake experiments.

A. Near-end SI cancellation

In this subsection, we investigate the digital SI cancellation performance in an indoor water tank and in a shallow lake.

1) Water tank experiment: In this experiment, we transmitted a Binary Phase Shift Keying (BPSK) modulated signal at a carrier frequency of $f_c = 24$ kHz with a frequency bandwidth of 1 kHz. RRC filters with a roll-off factor of 0.2 were used for pulse shaping and low-pass filtering. The sampling frequency was $f_s = 192$ kHz. The transmitted signal was 20 s in length, which included 5 s of zero-padding at the beginning of the transmission; the background noise level in the water tank was measured in this time period. In the tank experiment, the sliding-window RLS (SRLS) adaptive filter [21] was used for the SI cancellation. We used the base-band PA output as the regressor and the baseband hydrophone signal as the desired signal. The SI cancellation performance is evaluated by the steady-state normalized mean-squared error (NMSE). The NMSE at the ith time instant is computed as: $\text{NMSE}(i) = |e(i)|^2/P_x$, where $e(i)$ is the residual signal at the ith time instant, $P_x = \frac{1}{N}\sum_{i=1}^{N}|x(i)|^2$ is the average power of the desired signal, $x(i)$ is the desired signal sample and N is the number of samples in the desired signal. The parameters of the adaptive filter were as follows: the filter length $L = 80$ and the sliding window length $M = 1400$.

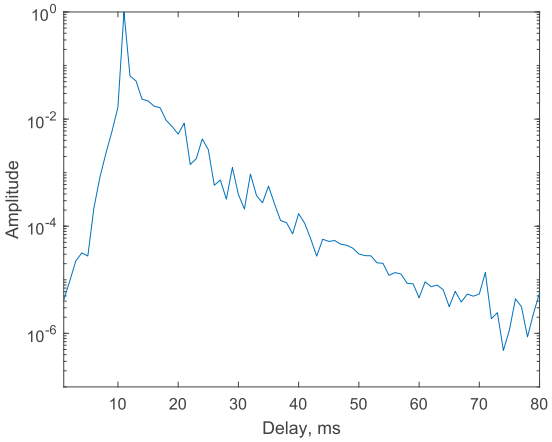

Fig. 3: Normalized estimate of the magnitude of the SI channel impulse response.

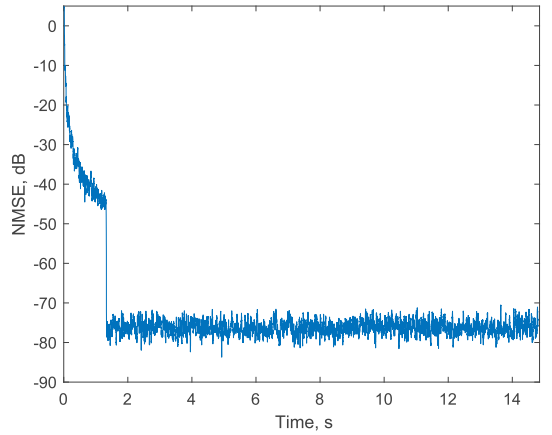

Fig. 4: Averaged NMSE performance of the SRLS algorithm.

The impulse response of the SI channel in the water tank is shown in Fig. 3. The sliding window length was selected to achieve the best NMSE performance. In Fig. 4, the NMSE performance of the SRLS algorithm is shown. To provide a better view of the NMSE performance, the NMSE curve has been smoothed by averaging the instantaneous NMSE over a period of 15 ms. The SI signal to noise ratio is 84.4 dB. With the aforementioned parameters, an average NMSE of -78.8 dB was achieved at the steady-state. This level of SI cancellation is high enough for FD communication. The gap between the NMSE level and the noise floor can be explained by the residual SI due to the long reverberation in the water tank.

2) Lake experiment: The experiment was conducted in a shallow lake. The maximum depth of the experimental site is around 1 m. During the experiment, the transducer was placed at around 0.5 m depth and fixed on an aluminium tube as shown in Fig. 5. We transmitted a BPSK signal at a carrier frequency of $f_c = 36$ kHz with 4 kHz frequency bandwidth. A higher carrier frequency was used in this experiment to avoid the high noise floor at lower frequencies. The SI to noise ratio in this experiment was 64.5 dB. As the true channel impulse

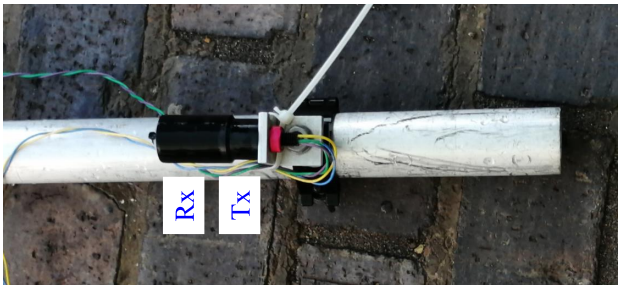

Fig. 5: Lake experiment FD tranducer.

response is not available, we used the (SI cancellation) SIC factor to evaluate the SI cancellation performance [22]. The SIC factor represents a ratio of the far-end SNR before and after SI cancellation (see details in [22]). In this experiment, the SIC factor was computed over a 10 s period after convergence of the adaptive filter.

As mentioned in Section III, the SI channel in practical scenarios contains both static paths (direct path, bottom reflections and reflections from static objects) and fast time-varying surface reflections. Although the surface reflections are much weaker compared to the static paths, they still need to be accurately estimated to cancel the SI. In such a scenario, the performance of the SRLS adaptive filter is limited. Therefore, for this experiment, the homotopy SRLS-L-DCD algorithm (HSRLS-L-DCD) was used due to its excellent tracking performance [6]. This adaptive filter exploits Legendre polynomials to approximate the channel time variations in vicinity of every time instant. It also exploits the SI channel impulse response sparseness. The adaptive filter length was set as $L = 150$ taps, which corresponded to a delay spread of 37.5 ms. The best SIC factor achieved with the SRLS algoirthm was 59.9 dB for the sliding window length at $M = 341$. We then applied the HSRLS-L-DCD algorithm with the following parameters: $M = 651$, the number of basis functions (Legendre polynomials) $P = 3$, the regularization parameter $\tau = 0.7$, the reweighting coefficient $\mu_w = 0.95$ and the parameter used for re-estimating the support $\mu_d = 7\times10^{-5}$ (see details in [6])). The complexity of the HSRLS-L-DCD algorithm is of $\mathcal{O}(P^2L^2)$ real-valued multiply and accumulate operations per sample. Analytical expression of the complexity is given in [6]. With the HSRLS-L-DCD algorithm, a SIC factor of 63.1 dB was achieved, which outperformed the SRLS algorithm by 3.2 dB.

The power spectra of the received signal before and after SI cancellation (using the HSRLS-L-DCD algorithm) and the background noise are shown in Fig. 6. To provide a clearer view, all the curves are smoothed by averaging over a frequency interval of 5 Hz. It can be seen that the residual signal was almost at the noise level after the SI cancellation.

B. Demodulation performance

In this subsection, we investigate the demodulation performance of the receiver in the lake experiments with the two-sensor transducer. The demodulation performance is evaluated by computing the bit error rate (BER).

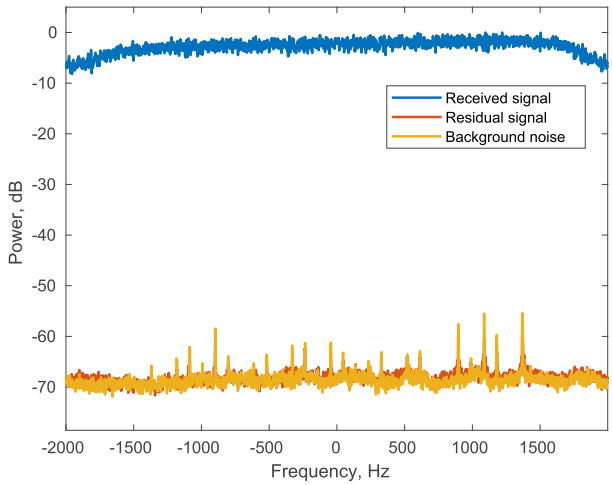

Fig. 6: Power spectra of the baseband signals in the lake experiment. The power spectral densities were normalized with respect to the maximum of the power spectral density of the received signal.

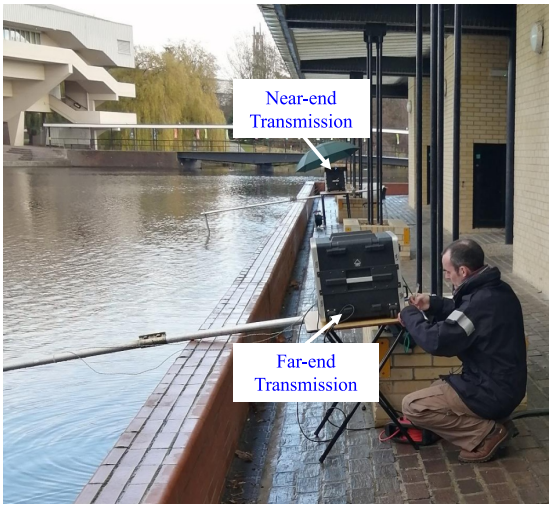

Fig. 7: Experimental setup of the FD experiment in the lake of the University of York.

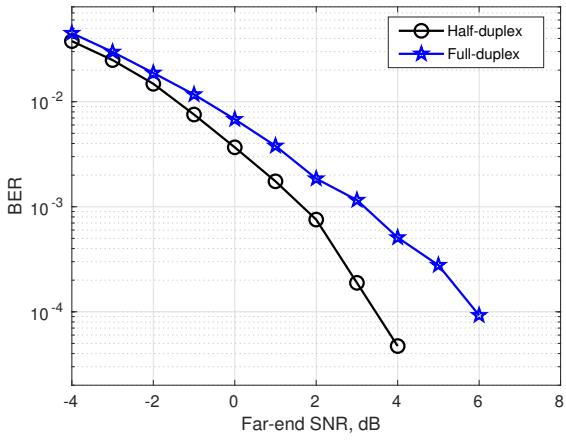

Fig. 8: Demodulation performance of the receiver in half-duplex and FD lake experiments.

In the lake experiments, 65 s of the far-end and near-end signals were transmitted. The near-end transmission used a BPSK signal at 36 kHz carrier frequency with 4 kHz bandwidth. For the far-end transmission, a spread-spectrum signal at the same carrier frequency and with the same bandwidth was transmitted. The far-end transmitted signal consists of superimposed binary pilot sequence (used for estimation of the far-end channel) and binary spread-spectrum data sequence with a spreading factor of 10; thus, the data rate is 400 bits per second. The far-end chip sequence was then pulse-shape filtered and up-shifted to the carrier frequency.

The experimental setup is shown in Fig. 7. Both the near-end and far-end transducers were fixed on metallic tubes and placed at around 0.5 m depth. We conducted two lake experiments. In the half-duplex experiment, only the far-end signal was transmitted. In the FD experiment, there was simultaneous near-end and far-end transmission. We used the same transmission power for the far-end transmission in these two experiments. The far-end SNR in both experiments was around 16 dB. To obtain demodulation performance at various far-end SNRs (SNR_{far}), complex-valued Gaussian random noise with variance σ_n^2 was added to the baseband received signal in both experiments, where σ_n^2 was computed as: $\sigma_n^2 = (P_s - P_n)/\mathrm{SNR}_{far} - P_n$, where P_s and P_n was the average power of the baseband far-end signal and background noise in the half-duplex experiment, respectively.

The first stage of the receiver is the digital SI cancellation. After SI cancellation, we obtain the far-end channel estimates by cross-correlating the pilot and the residual signal over 1 s duration. The Rake receiver is applied afterwards for maximal-ratio combining of signals arriving at the hydrophone over multipaths with different delays. We then proceed with the far-end data demodulation. As the focus of this paper is to demonstrate the feasibility of achieving FD UAC with the proposed two-sensor transducer, this simple receiver design was adopted. The BER performance of the receiver in half-duplex and FD lake experiments is shown in Fig. 8. For the FD experiment, the HSRLS-L-DCD algorithm was used for the digital SI cancellation. It can be seen that the loss of far-end SNR in the FD experiment was less than 3 dB compared to the half-duplex case.

V. Conclusion

In this paper we have presented a design of FD UAC receiver with a two-sensor FD transducer. The size of proposed two-sensor transducer is comparable with the conventional single-sensor transducer. Tank and lake experiments have been conducted to demonstate that the high level SI from the projector can be effectively cancelled by digital cancellation based on adaptive filtering. Both half-duplex and FD lake experiments have been conducted to evaluate the demodulation performance of the FD UAC receiver. Results indicated that there is a high potential of achieving FD communications with the proposed design.

Acknowledgement

For the purpose of open access, the authors have applied a CC BY license to any Accepted Manuscript version arising.

References

[1] M. Stojanovic and J. Preisig, "Underwater acoustic communication channels: Propagation models and statistical characterization," *IEEE Communications Magazine*, vol. 47, no. 1, pp. 84–89, 2009.

[2] D. Bliss, P. Parker, and A. Margetts, "Simultaneous transmission and reception for improved wireless network performance," in *IEEE/SP 14th Workshop on Statistical Signal Processing*, 2007, pp. 478–482.

[3] B. Radunovic, D. Gunawardena, P. Key, A. Proutiere, N. Singh, V. Balan, and G. Dejean, "Rethinking indoor wireless mesh design: Low power, low frequency, full-duplex," in *IEEE Workshop on Wireless Mesh Networks*, 2010, pp. 1–6.

[4] D. Korpi, T. Riihonen, V. Syrjälä, L. Anttila, M. Valkama, and R. Wichman, "Full-duplex transceiver system calculations: Analysis of ADC and linearity challenges," *IEEE Transactions on Wireless Communications*, vol. 13, no. 7, pp. 3821–3836, 2014.

[5] T. Yang, "Properties of underwater acoustic communication channels in shallow water," *The Journal of the Acoustical Society of America*, vol. 131, no. 1, pp. 129–145, 2012.

[6] L. Shen, Y. Zakharov, L. Shi, and B. Henson, "BEM adaptive filtering for SI cancellation in full-duplex underwater acoustic systems," *Signal Processing*, vol. 191, p. 108366, 2022.

[7] M. Towliat, Z. Guo, L. J. Cimini, X.-G. Xia, and A. Song, "Self-interference channel characterization in underwater acoustic in-band full-duplex communications using OFDM," in *IEEE Global Oceans 2020: Singapore–US Gulf Coast*, 2020, pp. 1–7.

[8] G. Qiao, S. Liu, Z. Sun, and F. Zhou, "Full-duplex, multi-user and parameter reconfigurable underwater acoustic communication modem," in *IEEE OCEANS-San Diego*, 2013, pp. 1–8.

[9] J. I. Choi, M. Jain, K. Srinivasan, P. Levis, and S. Katti, "Achieving single channel, full duplex wireless communication," in *Proceedings of the 16th Annual International Conference on Mobile Computing and Networking*, 2010, pp. 1–12.

[10] M. Jain, J. I. Choi, T. Kim, D. Bharadia, S. Seth, K. Srinivasan, P. Levis, S. Katti, and P. Sinha, "Practical, real-time, full duplex wireless," in *Proceedings of the 17th Annual International Conference on Mobile Computing and Networking*, 2011, pp. 301–312.

[11] B. King, J. Xia, and S. Boumaiza, "Digitally assisted RF-analog self interference cancellation for wideband full-duplex radios," *IEEE Transactions on Circuits and Systems II: Express Briefs*, vol. 65, no. 3, pp. 336–340, 2017.

[12] "Zoom F4 multitrack recorder," Accessed: 12th, April, 2022. [Online]. Available: https://zoomcorp.com/en/gb/handheld-video-recorders/field-recorders/f4-field-recorder/

[13] J. Tian, S. Yan, L. Xu, and J. Xi, "A time-reversal based digital cancelation scheme for in-band full-duplex underwater acoustic systems," in *IEEE OCEANS 2016-Shanghai*, 2016, pp. 1–4.

[14] G. Qiao, S. Gan, S. Liu, L. Ma, and Z. Sun, "Digital self-interference cancellation for asynchronous in-band full-duplex underwater acoustic communication," *Sensors*, vol. 18, no. 6, p. 1700, 2018.

[15] G. Qiao, S. Gan, S. Liu, and Q. Song, "Self-interference channel estimation algorithm based on maximum-likelihood estimator in in-band full-duplex underwater acoustic communication system," *IEEE Access*, vol. 6, pp. 62 324–62 334, 2018.

[16] L. Shen, B. Henson, Y. Zakharov, and P. Mitchell, "Digital self-interference cancellation for full-duplex underwater acoustic systems," *IEEE Transactions on Circuits and Systems II: Express Briefs*, vol. 67, no. 1, pp. 192–196, 2019.

[17] Niedźwiecki, A. Gańcza, L. Shen, and Y. Zakharov, "Adaptive identification of linear systems with a mix of static and time-varying parameters," *submitted to Signal Processing*, Preprint available at SSRN: http://dx.doi.org/10.2139/ssrn.4076753.

[18] J. Proakis and M. Salehi, *Digital Communications*. McGraw-Hill, 2008.

[19] Y.-T. Hsieh, M. Rahmati, and D. Pompili, "FD-UWA: Full-duplex underwater acoustic comms via self-interference cancellation in space," in *2020 IEEE 17th International Conference on Mobile Ad Hoc and Sensor Systems (MASS)*. IEEE, 2020, pp. 256–264.

[20] "Piezo ceramic cylinder, Steniner and Martins, Inc," Accessed: 11th, April, 2022. [Online]. Available: https://www.steminc.com/PZT/en/piezo-ceramic-cylinder-26x22x13mm-43-khz

[21] S. Haykin, *Adaptive Filter Theory*. Prentice Hall, 2002.

[22] L. Shen, Y. Zakharov, B. Henson, N. Morozs, and P. D. Mitchell, "Adaptive filtering for full-duplex UWA systems with time-varying self-interference channel," *IEEE Access*, vol. 8, pp. 187 590–187 604, 2020.